Electronic Supplementary Material (ESI) for Green Chemistry.
This journal is © The Royal Society of Chemistry 2022

Supporting Information

Cocrystal Engineering Strategy for Sustained Release and Leaching Reduction of Herbicides: A Case Study of Metamitron

Yuntian Xiao[a], Chuanhua Wu[a], Ling Zhou[a,b,c], Qiuxiang Yin[a,b,c,], Jingxiang Yang[d,*]*

[a] *School of Chemical Engineering and Technology, Tianjin University, Tianjin 300072, People's Republic of China.*

[b] *Collaborative Innovation Center of Chemical Science and Engineering (Tianjin), Tianjin 300072, China.*

[c] *State Key Laboratory of Chemical Engineering, Tianjin University, Tianjin 300072, People's Republic of China.*

[d] *State Key Laboratory of Elemento-Organic Chemistry and Department of Chemical Biology, College of Chemistry, Nankai University, Tianjin 300071, China*

Contents

Table S1. Overview of Screening Experiments

Table S2. HPLC method parameters for MET

Table S3. Physical and chemical parameters of the soil column

Table S4. UPLC method parameters for MET

Table S5. Hydrogen bond geometrical parameters of cocrystals

Table S6. Summary tables of significance analysis of leaching behavior

Table S7. Analysis of significant differences between different cocrystal treatment groups

Table S8. Relevant properties such as soil pH and CEC after all kinds of herbicides have been applied.

Figure S1. Standard curve of MET content (concentration-peak area) determined by HPLC.

Figure S2. Schematic diagram of the soil column experiment.

Figure S3. Standard curve of MET content (concentration-peak area) determined by UPLC.

Figure S4. Supramolecular synthons with similar structures reported in the literature.

Figure S5. PXRD pattern of the MET-CA neat grinding product (yellow) compared with MET (blue), CA (orange) and the calculated pattern obtained from the single crystal data (purple).

Figure S6. PXRD pattern of the MET-NA neat grinding product (yellow) compared with MET (blue), NA (orange) and the calculated pattern obtained from the single crystal data (purple).

Figure S7. PXRD pattern of the MET-BA neat grinding product (yellow) compared with MET (blue), BA (orange) and the calculated pattern obtained from the single crystal data (purple).

Figure S8. Confocal Raman micro-spectra of the MET-CA neat grinding product (yellow) compared MET (blue) and CA (orange).

Figure S9. Confocal Raman micro-spectra of the MET-NA neat grinding product (yellow) compared MET (blue) and NA (orange).

Figure S10. Confocal Raman micro-spectra of the MET-CA neat grinding product (yellow) compared MET (blue) and BA (orange).

Figure S11. Comparison of DSC plots of MET (blue) and CA (orange) with the MET-CA cocrystal (yellow).

Figure S12. Comparison of DSC plots of MET (blue) and NA (orange) with the MET-NA cocrystal (yellow).

Figure S13. Comparison of DSC plots of MET (blue) and BA (orange) with the MET-BA cocrystal (yellow).

Figure S14. The TGA traces of MET (blue) and CA (orange) with the MET-CA cocrystal (yellow).

Figure S15. The TGA traces of MET (blue) and NA (orange) with the MET-NA cocrystal (yellow).

Figure S16. The TGA traces of MET (blue) and BA (orange) with the MET-BA cocrystal (yellow).

Figure S17. PXRD patterns of all cocrystals under accelerated storage conditions (40 °C, 75% RH) over 9 weeks. (a) MET-CA, (b) MET-NA, and (c) MET-BA.

Figure S18. PXRD patterns of MET and cocrystals after 48h suspension in water at 25 °C.

Figure S19. PXRD patterns of MET and cocrystals after 48h suspension in water at 35 °C.

Figure S20. PXRD patterns of MET and cocrystals after 48h suspension in water at 45 °C.

Figure S21. Dissolution profiles of MET, and three cocrystals in water at 35 °C.

Figure S22. Dissolution profiles of MET, and three cocrystals in water at 45 °C.

Figure S23. Morphological pictures of Kentucky bluegrass after 14 days of different treatments (data represent germination rate).

Supporting Tables:

Table S1. Overview of Screening Experiments

Agrichemical name	Coformer name	Result
Metamitron	Cinnamic acid	√√
Metamitron	Ferulic acid	×
Metamitron	Syringic acid	×
Metamitron	Vanillic acid	×
Metamitron	P-coumaric acid	×
Metamitron	Hesperetin	×
Metamitron	Gallic acid	×
Metamitron	Salicylic acid	×
Metamitron	Ellagic acid	×
Metamitron	Quercetin	×
Metamitron	Hesperetin	×
Metamitron	Kaempferol	×
Metamitron	Baicalein	√√
Metamitron	Resveratrol	√
Metamitron	Naringenin	√√
Metamitron	Catechins	×
Metamitron	Glycolic acid	×

√ represents a new cocrystal/salt determined by PXRD; √√ represents a new cocrystal/salt determined by PXRD and its structure is determined by SCXRD; × represents no new cocrystal/salt found by PXRD

Table S2. HPLC method parameters for MET

Parameter	Details
System	Agilent 1260 LC
Column	C18 column (6 μm, 4.6 mm × 150 mm)
Mobile phase	Methanol-water (70:30)
Flow rate	1 mL/min
Inject volume	20 μL
Column temperature	25 °C
Sample temperature	25 °C
λ_{max}	254 nm
Retention time	4.6 min
Equation	y = 22311.5587x + 21.10418
Regression coefficient (R^2)	0.99999
Calibration range	0.01 – 0.4 mg/mL

Table S3. Physical and chemical parameters of the soil column

Properties	Indicators
Soli particle size (mm)	≤ 2
Weight (g)	250
Volumetric weight (g/cm^3)	1.29 ± 0.02
Loading height (cm）	16.0 ± 0.3
Pore volume (mL)	116.2 ± 3.1
Flow velocity (mL/min)	1.0

Table S4. UPLC method parameters for MET

Parameter	Details
System	Waters ACQUITY
Column	C18 column (6 μm, 4.6 mm × 150 mm)
Mobile phase	Methanol-water (70:30)
Flow rate	1 mL/min
Inject volume	20 μL
Column temperature	25 °C
Sample temperature	25 °C
λ_{max}	254 nm
Retention time	4.2 min
Equation	y = 111.1247x + 0.35979
Regression coefficient (R^2)	0.99998
Calibration range	0.1 – 1.0 μg/mL

Table S5. Hydrogen bond geometrical parameters of cocrystals

Compound	D–H···A	d(H···D)/Å	d(H···A)/Å	d(D···A)/Å	θ(D–H···A)/°	symmetry code
MET-CA	N(4)-H(4A)···N(1)	0.865	2.481	3.121	131.34	x+1/2, -y+3/2, z+1/2
	N(4)-H(4A)···O(3)	0.865	2.397	3.012	128.51	x+1/2, -y+3/2, z+1/2
	N(4)-H(4B)···O(1)	0.924	2.209	2.698	112.26	x-1,y,z
	N(4)-H(4B)···O(6)	0.924	2.453	3.189	136.67	x+2, y, z+1
	O(2)-H(2)···N(2)	0.840	1.828	2.656	168.41	

	N(8)-H(8A)···O(3)	0.860	2.291	3.037	145.12	
	N(8)-H(8A)···O(4)	0.860	2.264	2.688	110.39	
	O(5)-H(5)···N(6)	0.840	1.857	2.683	167.21	
MET-NA	N(1)-H(1A) ···O(6)	0.865	2.213	2.902	136.43	x+1, -y+1, z+1/2
	N(1)-H(1B)···O(4)	0.865	2.126	2.869	143.70	x, y+1, z
	O(2)-H(2)···N(3)	0.840	1.811	2.632	165.37	
	O(3)-H(3)···O(4)	0.840	1.846	2.586	146.24	
	O(3)-H(3)···O(6)	0.840	2.540	3.042	119.48	x+1, -y, z+1/2
	O(6)-H(6)···O(3)	0.840	1.922	2.734	162.21	x-1, y, z-1
MET-BA	N(4)-H(4A)···O(1)	0.945	2.219	2.709	111.31	
	N(4)-H(4A)···O(3)	0.945	2.376	3.223	149.00	-x+3/2, y+1/2, -z+3/2
	N(4)-H(4B)···O(2)	0.961	2.002	2.954	170.83	-x+1/2, y+1/2, -z+3/2
	O(2)-H(2B)···O(6)	0.894	1.715	2.560	156.64	
	O(3)-H(3B)···O(1)	0.891	1.976	2.782	149.56	-x+3/2, y-1/2, -z+3/2
	O(3)-H(3B)···O(4)	0.891	2.189	2.678	113.94	
	O(4)-H(4C)···N(2)	0.952	2.623	3.519	157.00	
	O(4)-H(4C)··· N(1)	0.952	1.725	2.673	173.54	

Table S6. Summary tables of significance analysis of leaching behavior

MET - CA：

Analysis of variance: one-way analysis of variance

SUMMARY

Groups	*Counts*	*Sum*	*Average*	*Variance*
Column 1	12	1053.86658	87.822215	437.199827

		9	7	4
Column 2	12	850.0352102	70.83626675	939.4982109

ANOVA

Source of Variation	*SS*	*df*	*MS*	*F*	***P-value***	*F crit*
Between Groups	1731.134619	1	1731.13462	2.514908239	**0.127044**	4.30095
With Groups	15143.67842	22	688.3490199			
Total	16874.81304	23				

MET - NA：

Analysis of variance: one-way analysis of variance

SUMMARY

Groups	*Counts*	*Sum*	*Average*	*Variance*
Column 1	12	1053.867	87.82222	437.1998
Column 2	12	97.84546	8.153788	43.03884

ANOVA

Source of Variation	*SS*	*df*	*MS*	*F*	***P-value***	*F crit*
Between Groups	38082.35	1	38082.35	158.5976	**1.56E-11**	4.30095
With Groups	5282.625	22	240.1193			
Total	43364.98	23				

MET - BA：

Analysis of variance: one-way analysis of variance

SUMMARY

Groups	*Counts*	*Sum*	*Average*	*Variance*
Column 1	12	1053.867	87.82222	437.1998
Column 2	12	165.6016	13.80014	85.86715

ANOVA

Source of Variation	*SS*	*df*	*MS*	*F*	***P-value***	*F crit*
Between Groups	32875.61	1	32875.61	125.7033	**1.45E-10**	4.30095
With Groups	5753.737	22	261.5335			
Total	38629.35	23				

Table S7. Analysis of significant differences between different cocrystal treatment groups

Post Hoc Tests

Homogeneous Subsets

Duncan

treatment	N	Subset for alpha = 0.05		
		1	2	3
MET	74	3.4789		
MET-CA	72	4.8593		
MET-BA	74		66.9409	
MET-NA	71			82.1775
Sig.		0.823	1.000	1.000

Table S8. Relevant properties such as soil pH and CEC after all kinds of herbicides have been applied.

Compound	pH	CEC [mmol/kg]
MET	6.95±0.16	171±4
MET-CA	6.89±0.12	182±2
MET-NA	7.06±0.01	174±11
MET-BA	7.04±0.12	181±7

Supporting Figures:

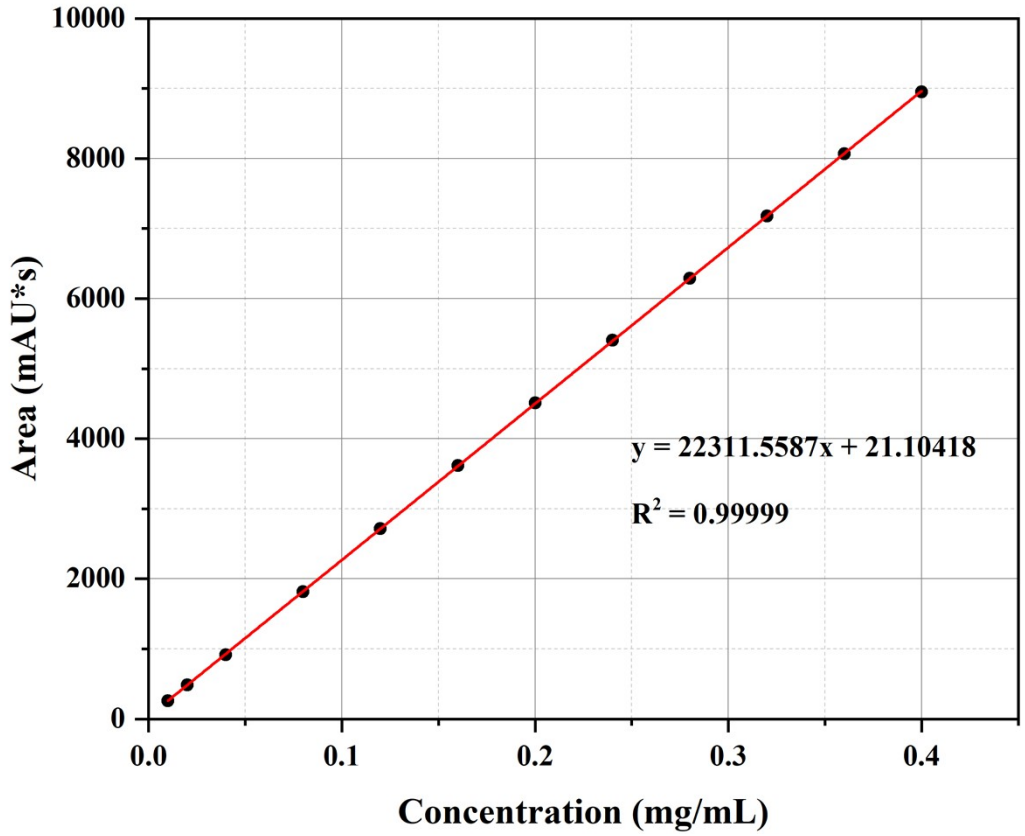

Figure S1. Standard curve of MET content (concentration-peak area) determined by HPLC.

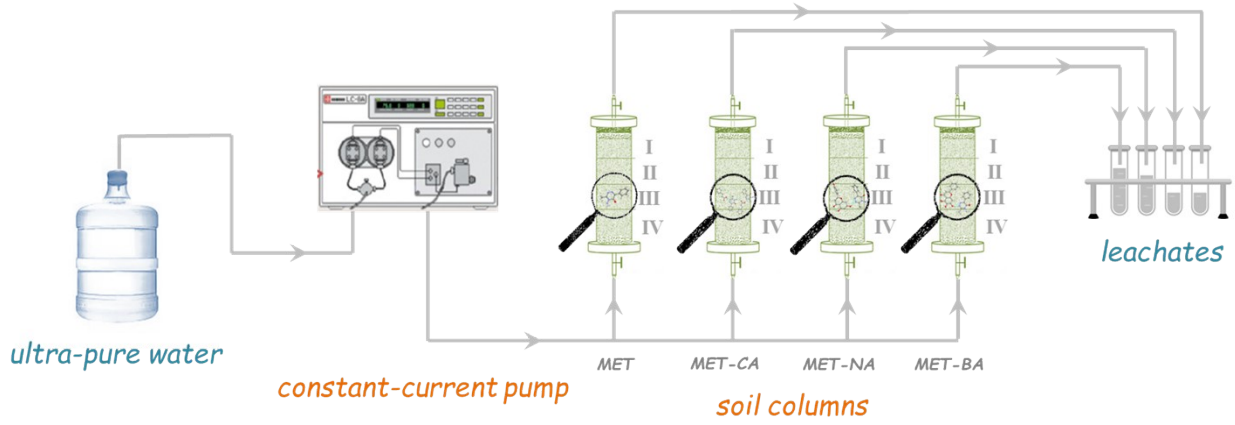

Figure S2. Schematic diagram of the soil column experiment.

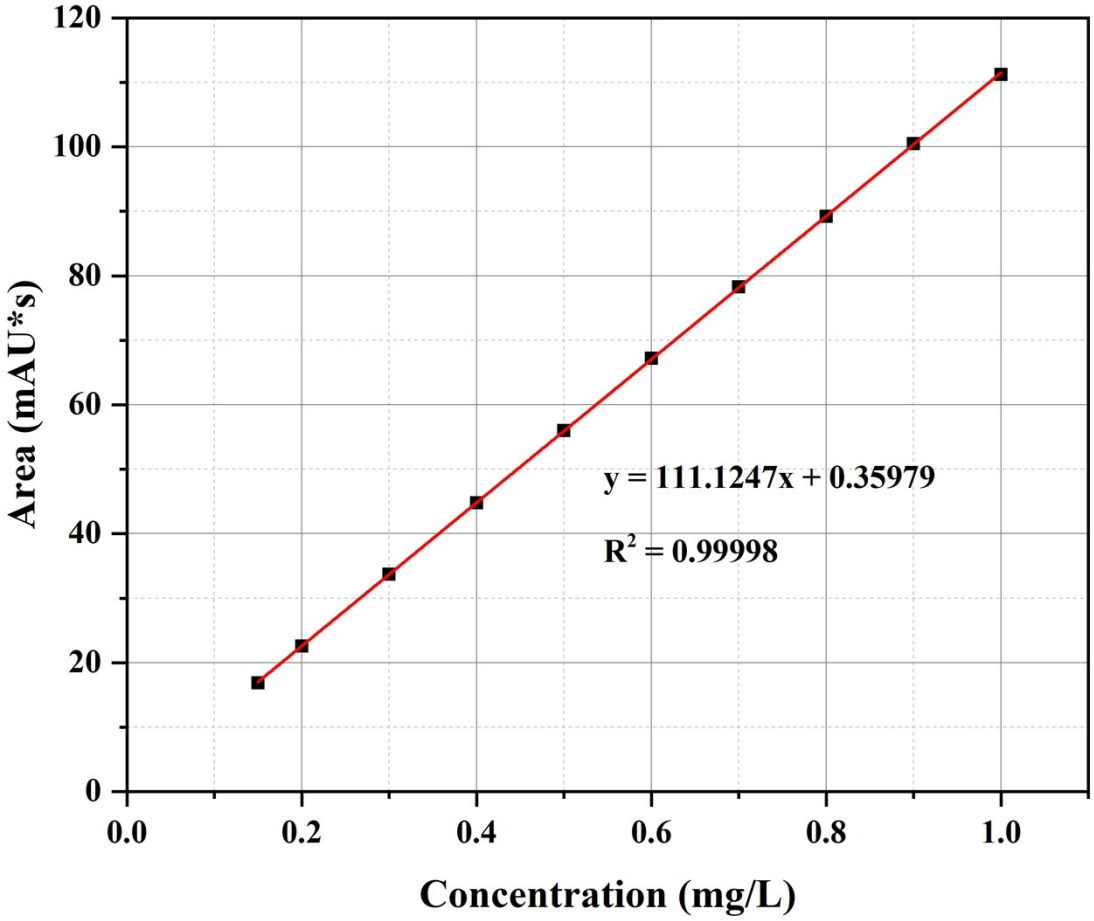

Figure S3. Standard curve of MET content (concentration-peak area) determined by UPLC.

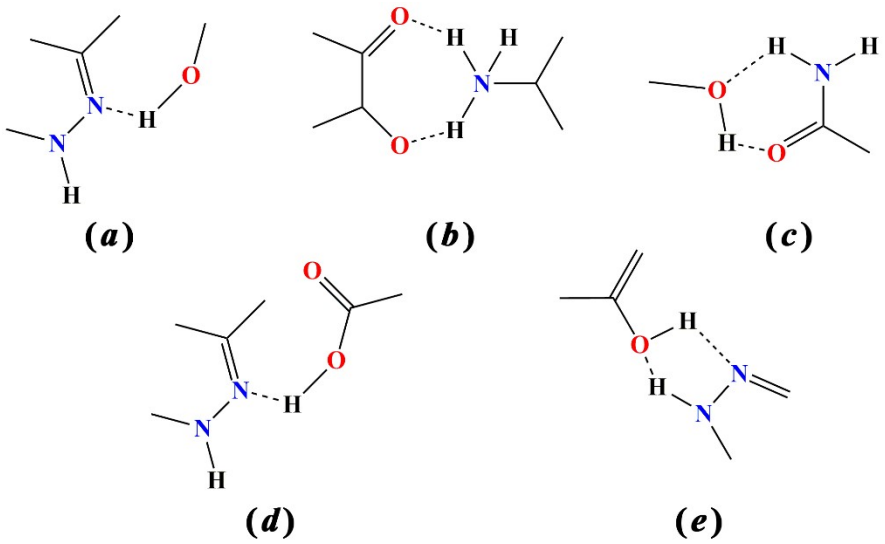

Figure S4. Supramolecular synthons with similar structures reported in the literature.[1-9]

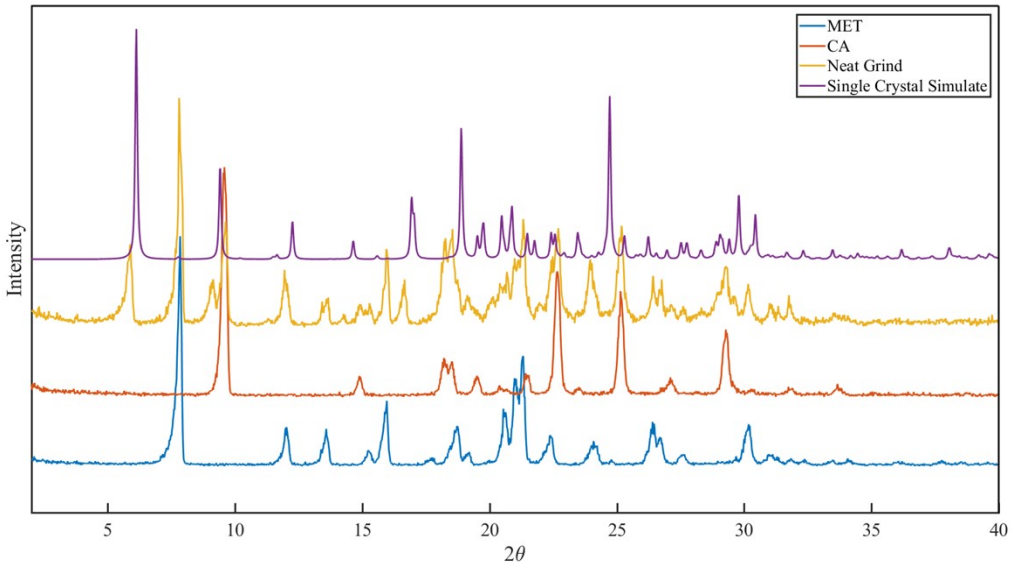

Figure S5. PXRD pattern of the MET-CA neat grinding product (yellow) compared with MET (blue), CA (orange) and the calculated pattern obtained from the single crystal data (purple).

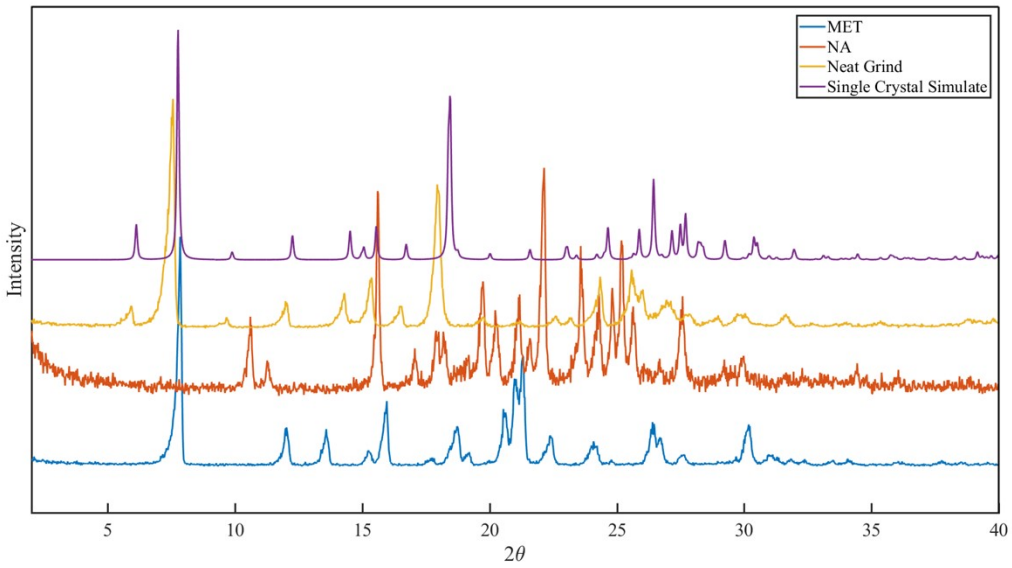

Figure S6. PXRD patterns of the MET-NA neat grinding product (yellow) compared with MET (blue), NA (orange) and the calculated pattern obtained from the single crystal data (purple).

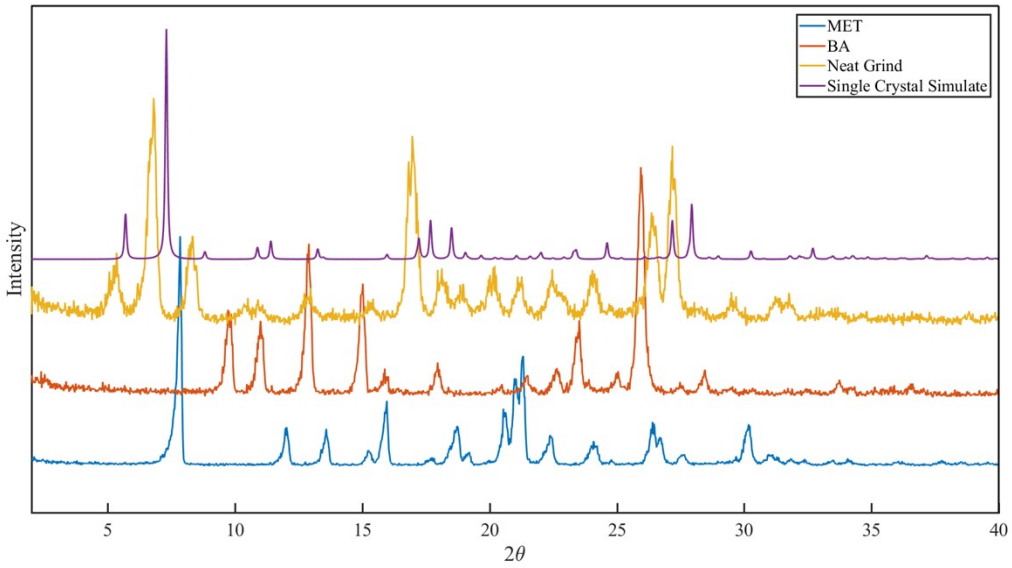

Figure S7. PXRD pattern of the MET-NA neat grinding product (yellow) compared with MET (blue), NA (orange) and the calculated pattern obtained from the single crystal data (purple).

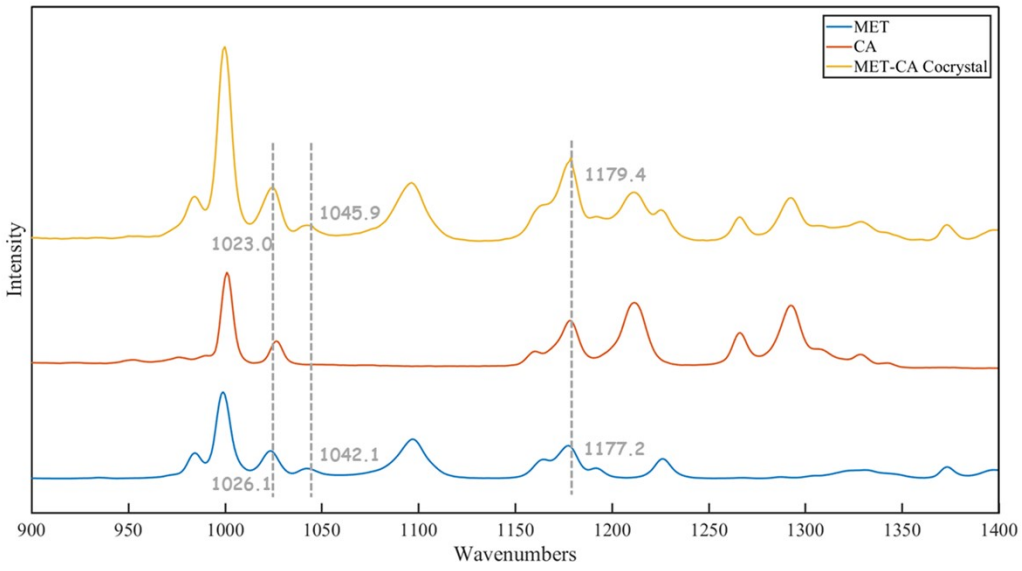

Figure S8. Confocal Raman micro-spectra of the MET-CA neat grinding product (yellow) compared MET (blue) and CA (orange).

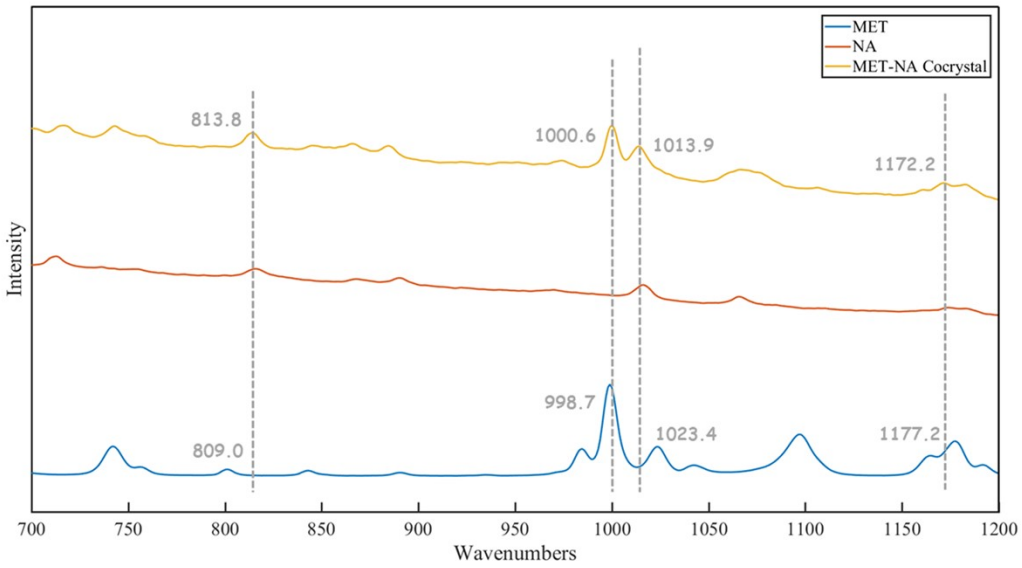

Figure S9. Confocal Raman micro-spectra of the MET-NA neat grinding product (yellow) compared MET (blue) and NA.

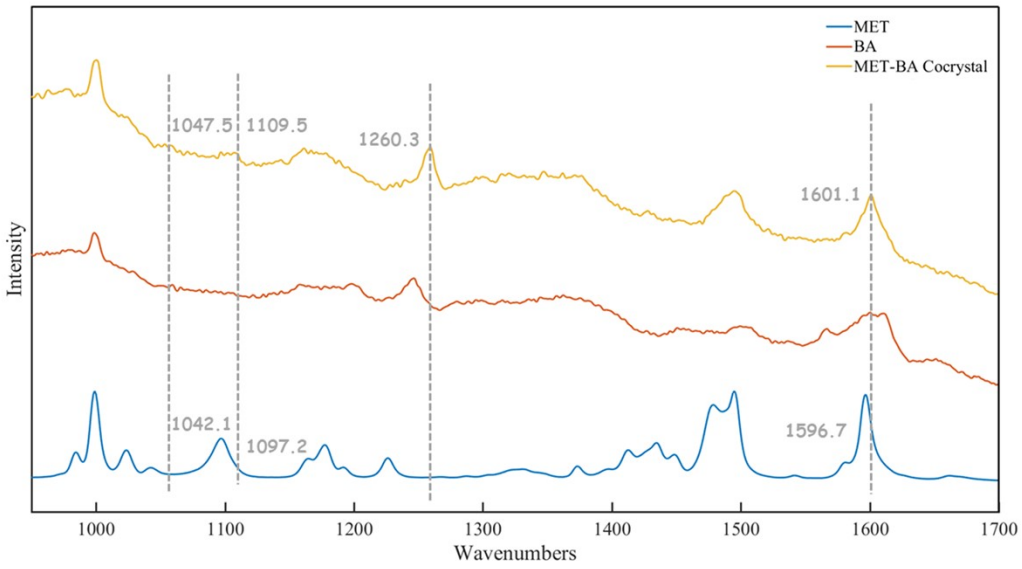

Figure S10. Confocal Raman micro-spectra of the MET-BA neat grinding product (yellow) compared MET (blue) and BA (orange).

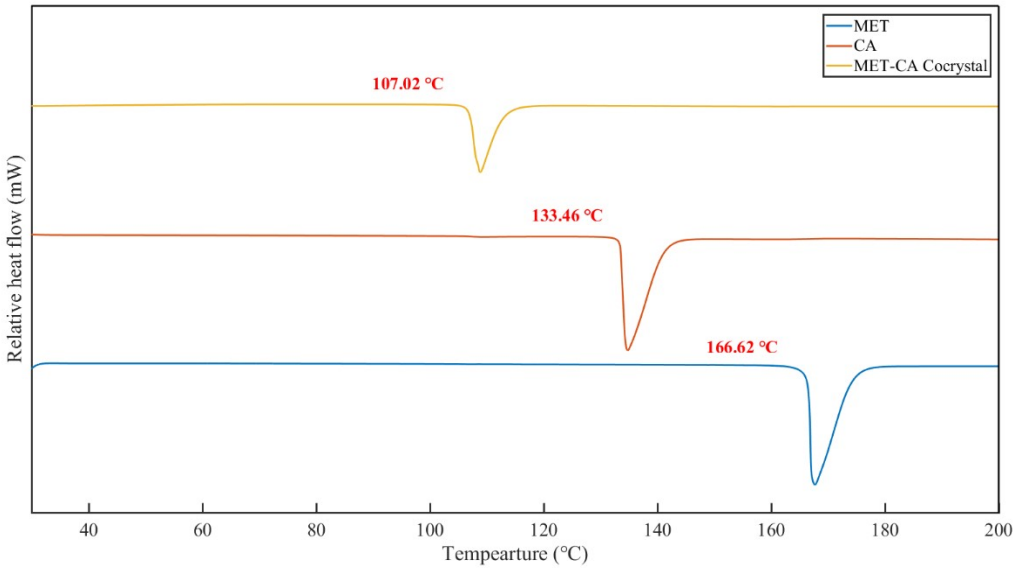

Figure S11. Comparison of DSC plots of MET (blue) and CA (orange) with the MET-CA cocrystal (yellow).

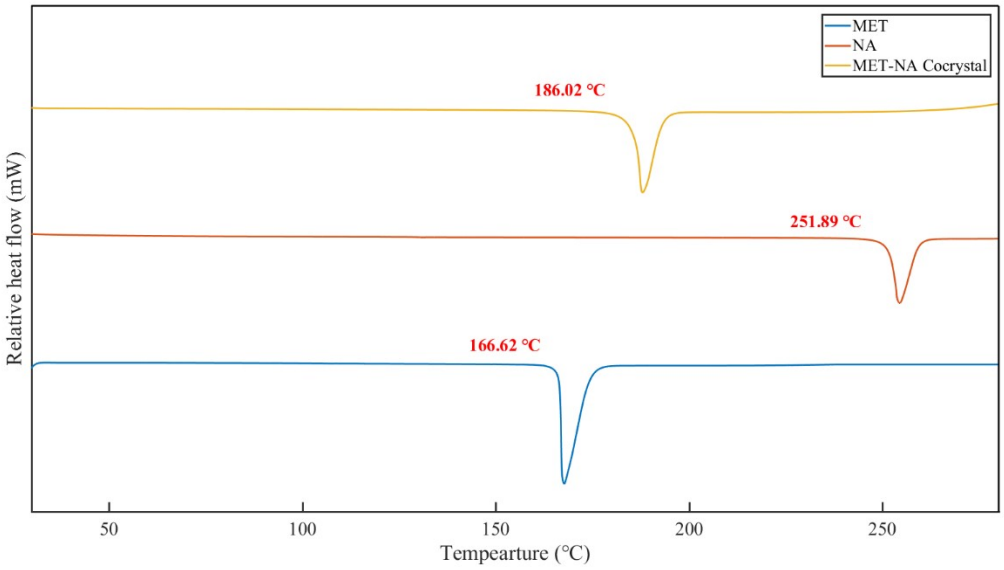

Figure S12. Comparison of DSC plots of MET (blue) and CA (orange) with the MET-NA cocrystal (yellow).

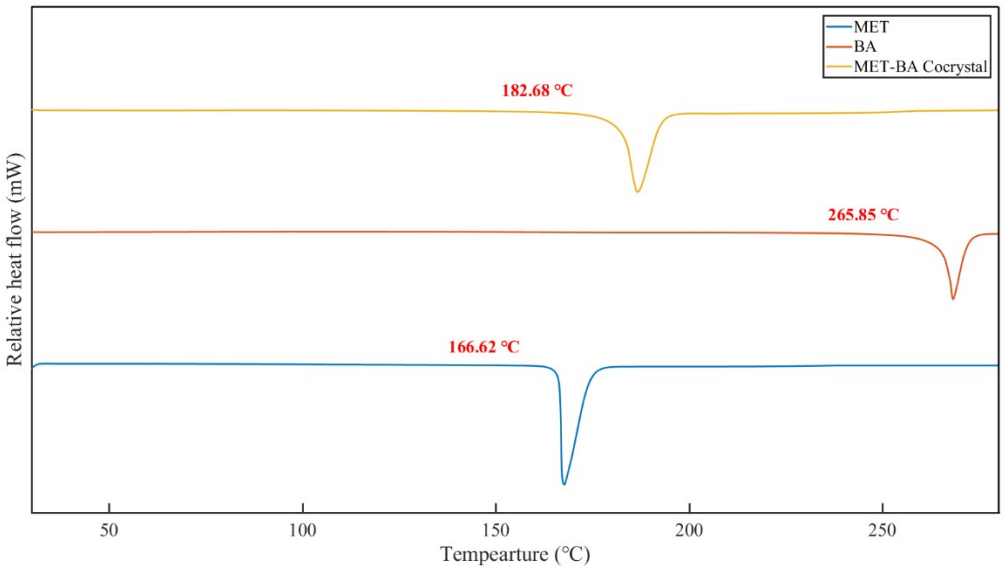

Figure S13. Comparison of DSC plots of MET (blue) and CA (orange) with the MET-BA cocrystal (yellow).

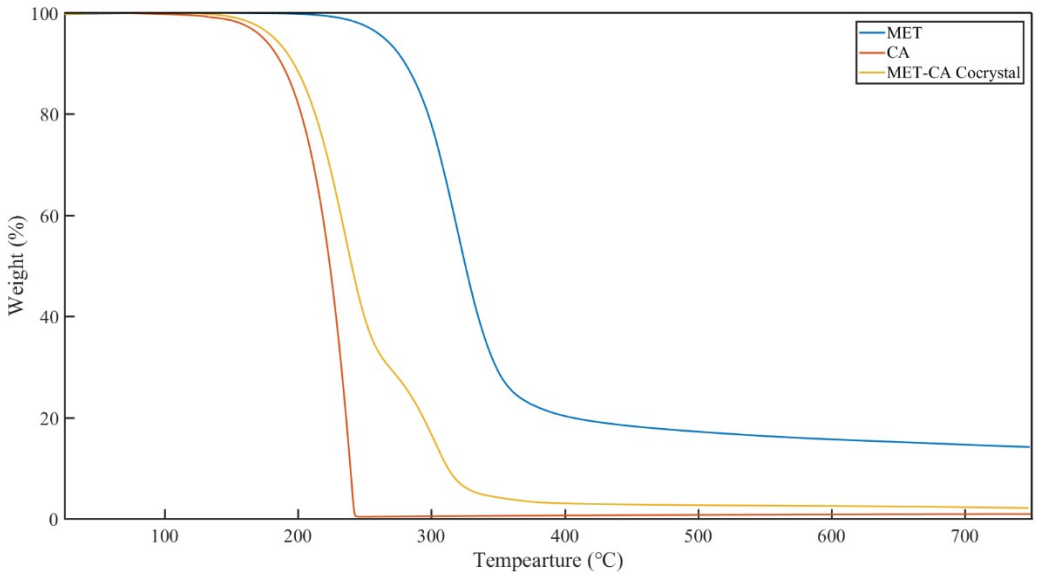

Figure S14. The TGA traces of MET (blue) and CA (orange) with the MET-CA cocrystal (yellow).

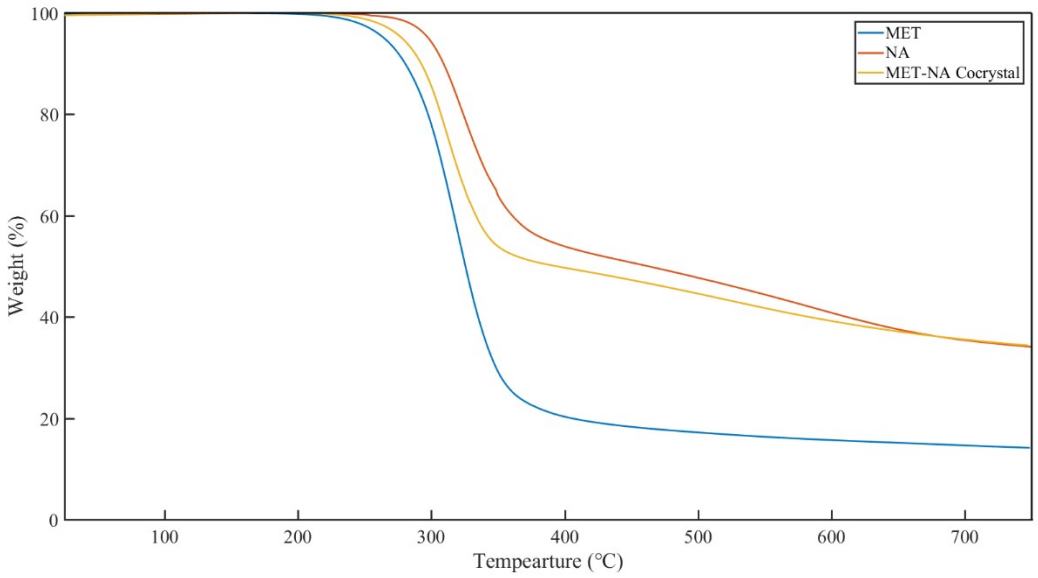

Figure S15. The TGA traces of MET (blue) and NA (orange) with the MET-NA cocrystal (yellow).

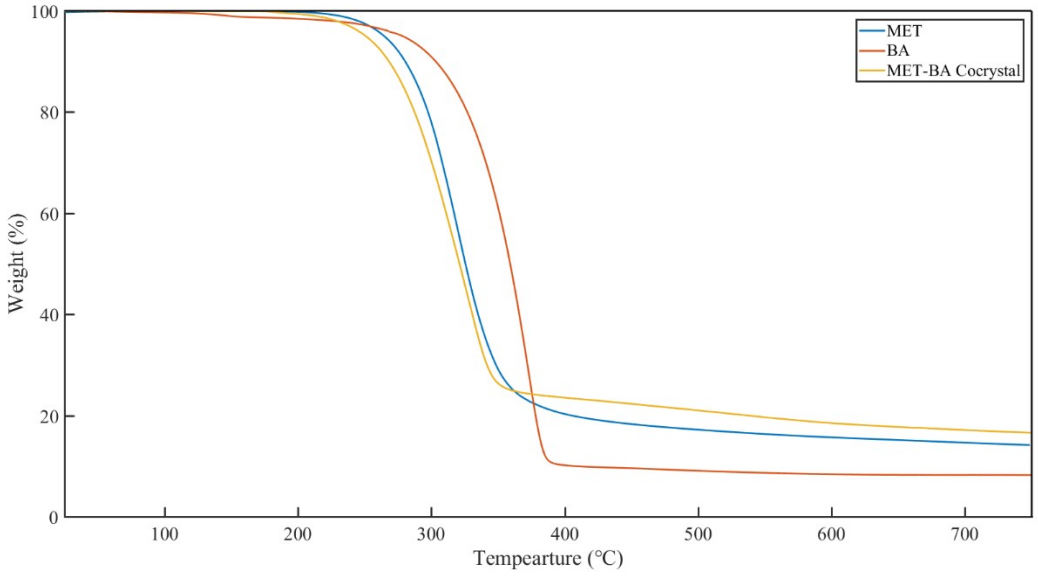

Figure S16. The TGA traces of MET (blue) and BA (orange) with the MET-BA cocrystal (yellow).

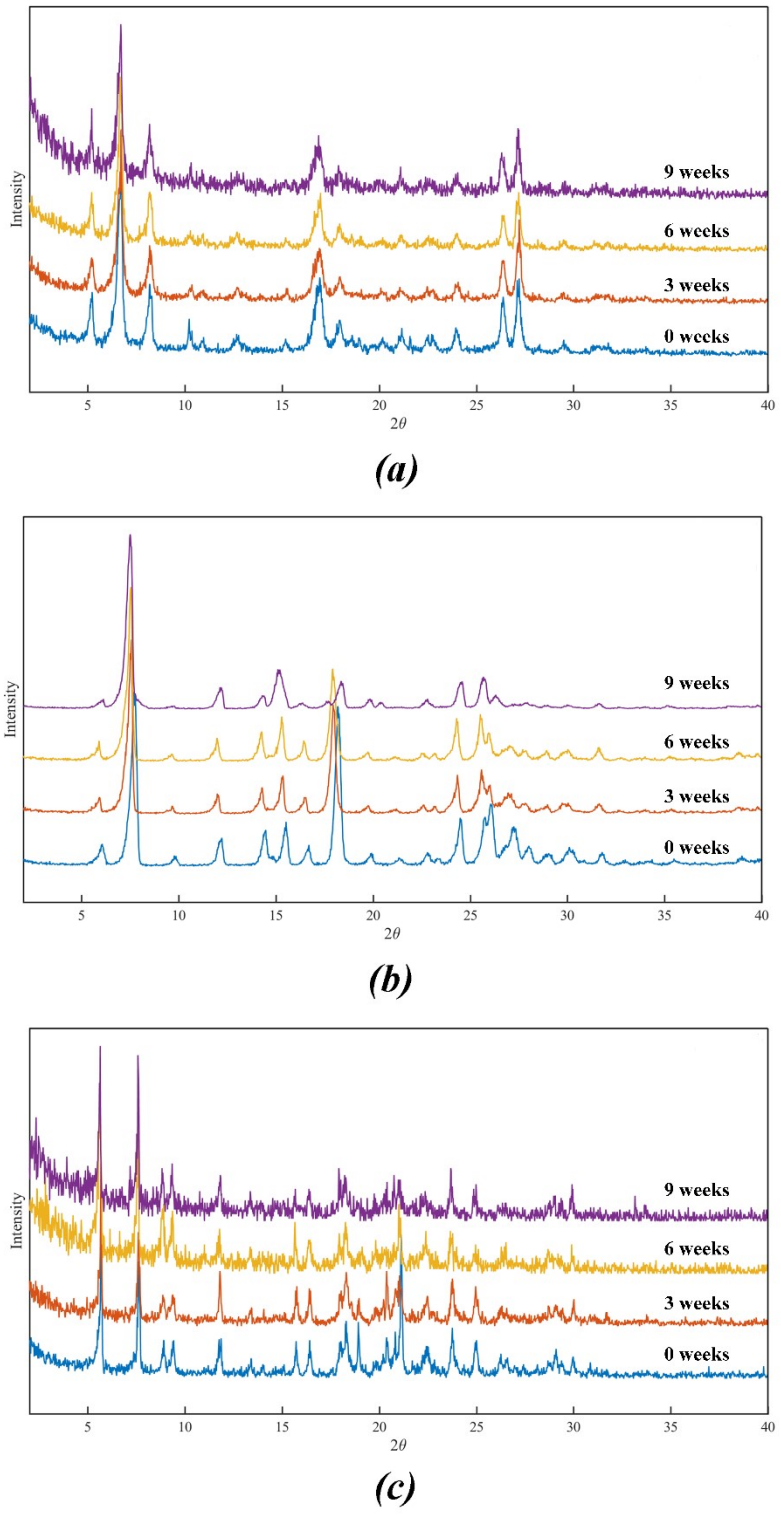

Figure S17. PXRD patterns of all cocrystals under accelerated storage conditions (40 °C, 75% RH) over 9 weeks. (a) MET-CA, (b) MET-NA, and (c) MET-BA.

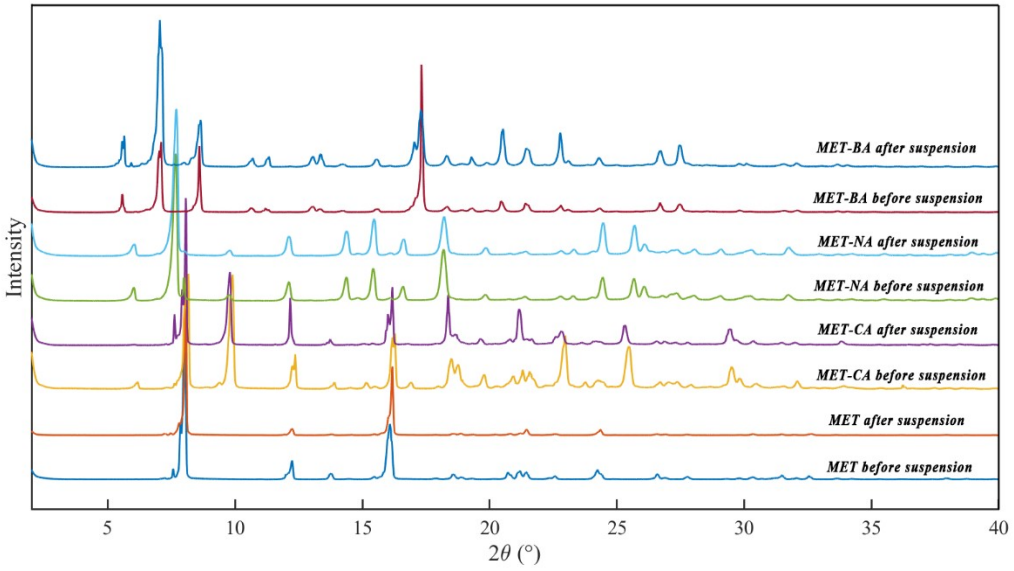

Figure S18. PXRD patterns of MET and cocrystals after 48 h suspension in water at 25 °C.

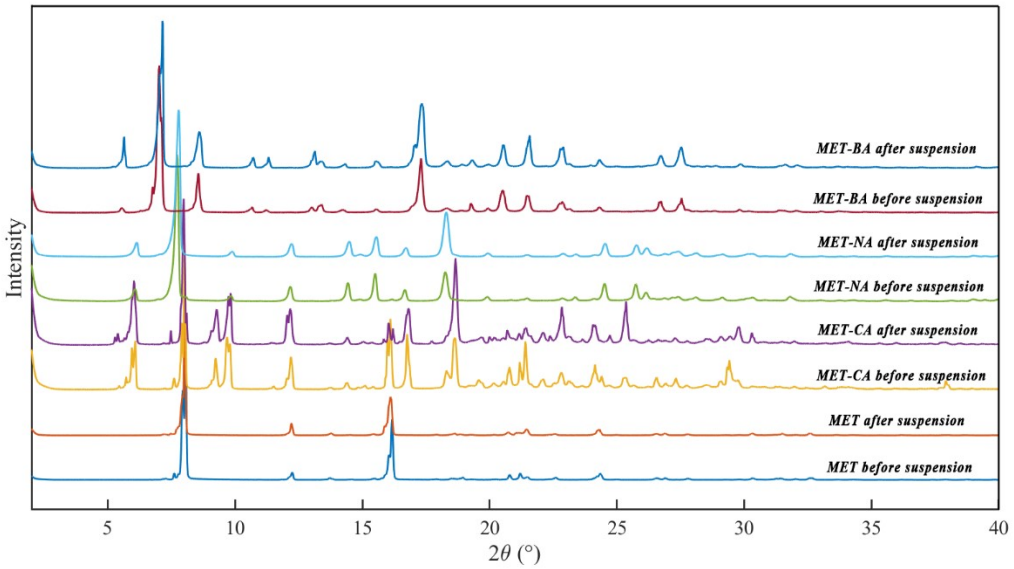

Figure S19. PXRD patterns of MET and cocrystals after 48 h suspension in water at 35 °C.

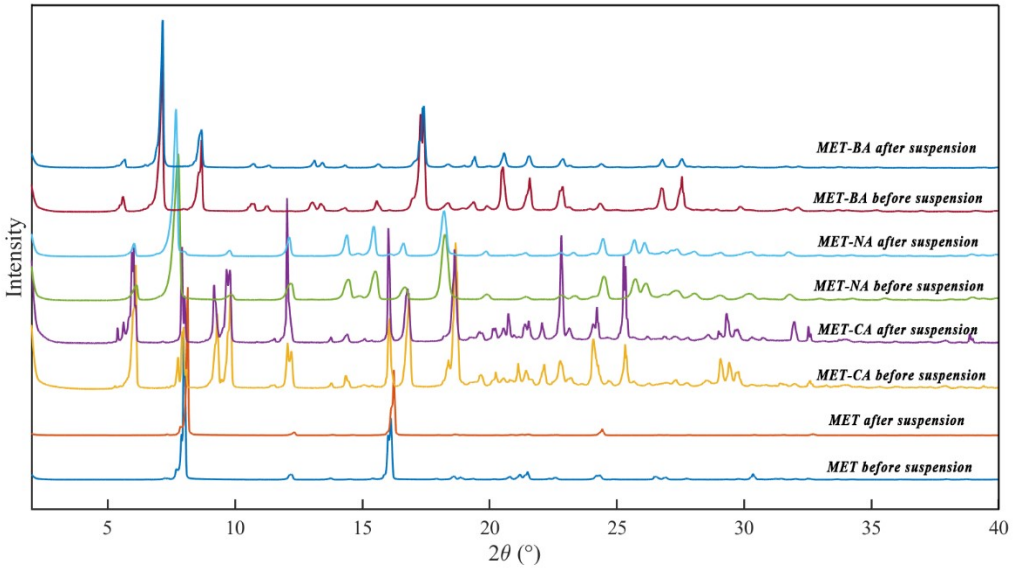

Figure S20. PXRD patterns of MET and cocrystals after 48 h suspension in water at 45 °C.

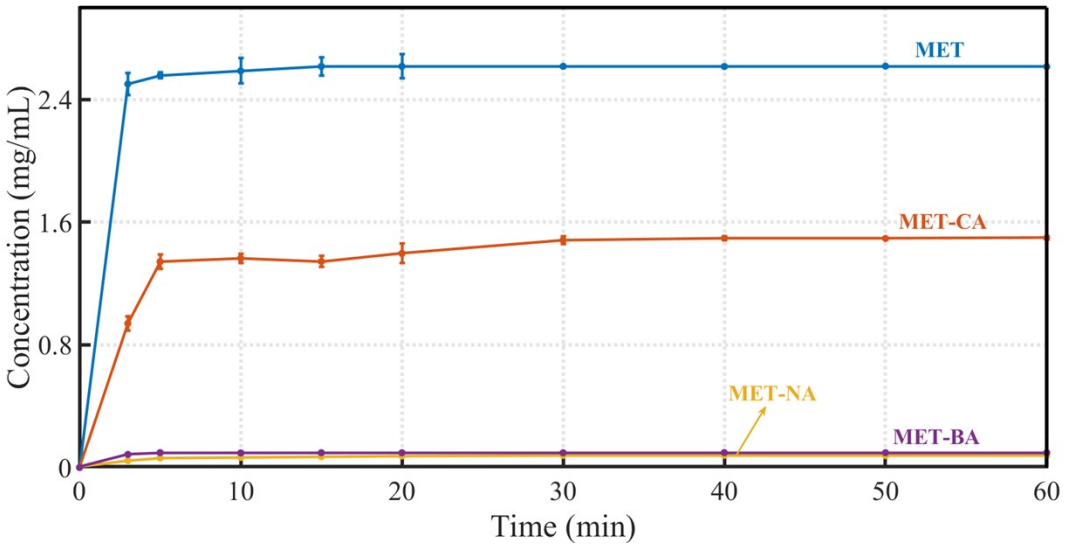

Figure S21. Dissolution profiles of MET, and three cocrystals in water at 35 °C.

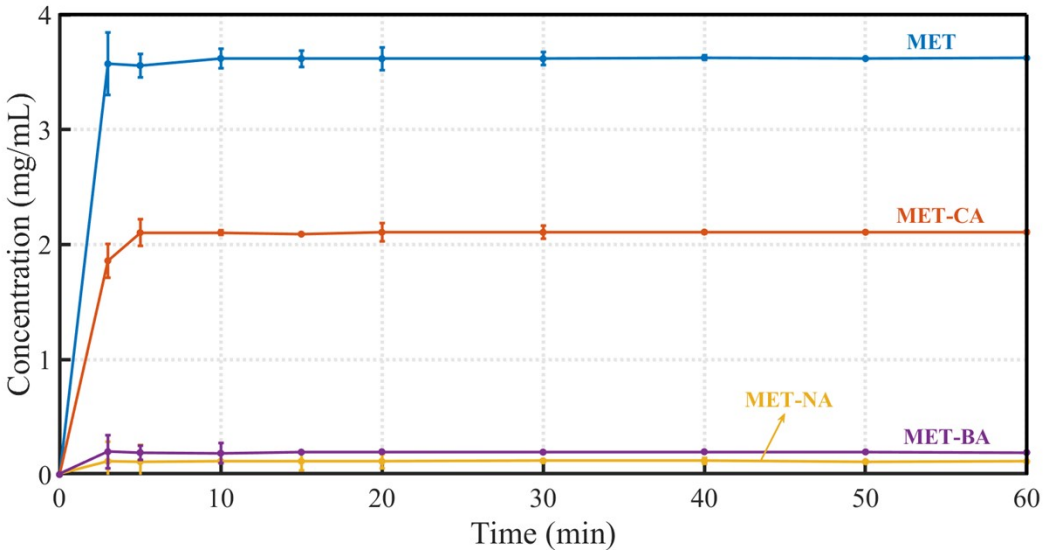

Figure S22. Dissolution profiles of MET, and three cocrystals in water at 45 °C.

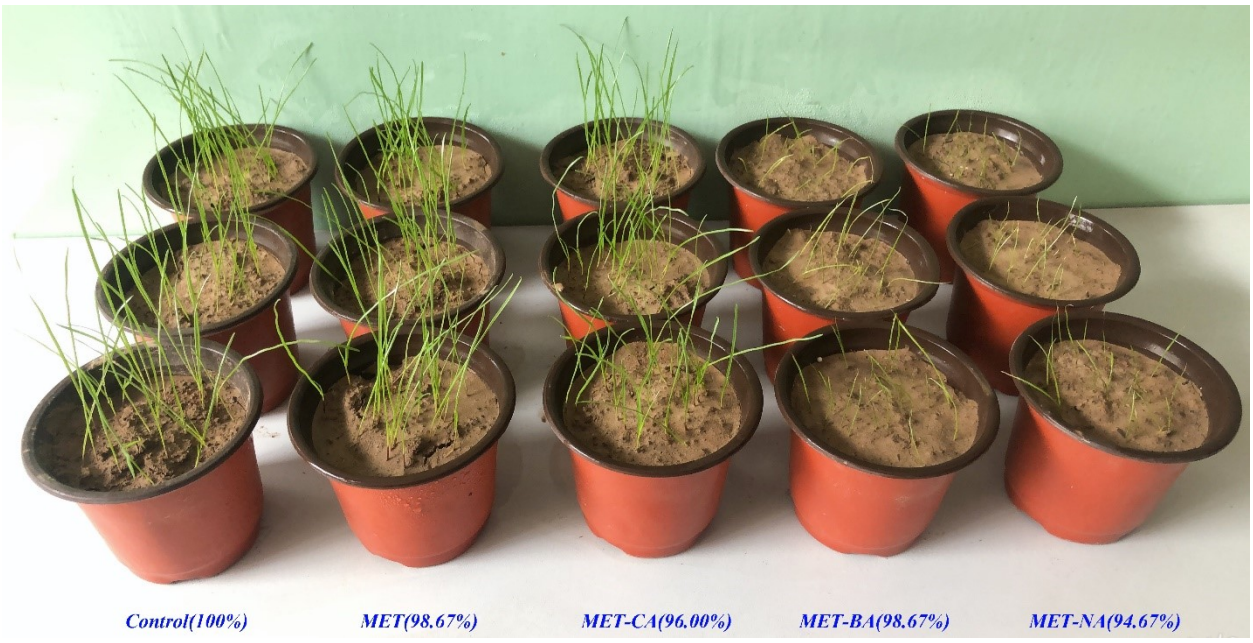

Figure S23. Morphological pictures of Kentucky bluegrass after 14 days of different treatments (data represent germination rate: Control, 100%; MET, 98.67%; MET-CA, 96.00%; MET-BA, 98.67%; MET-NA, 94.67%).

References:

1 Y. Yang, W. Tang, S. Liu, D. Han, Y. Liu and J. Gong, *J. Mol. Liq*., 2017, 243, 472-483.

2 J. Sui, Y. Luo, J. Zhai, F. Fan, L. Zhang, J. Lu and X. Zhu, *J. Mol. Liq*., 2020, 304, 112723.

3 D. Wu, J. Li, Y. Xiao, X. Ji, C. Li, B. Zhang, B. Hou, L. Zhou, C. Xie and J. Gong, *Cryst. Growth Des*., 2021, 21, 2371-2388.

4 K. Suresh, V. S. Minkov, K. K. Namila, E. Derevyannikova, E. Losev, A. Nangia and E. V. Boldyreva, *Cryst. Growth Des*., 2015, 15, 3498-3510.

5 Y. Yuan, D. Li, C. Wang, S. Chen, M. Kong, Z. Deng, C. C. Sun and H. Zhang, *Cryst. Growth Des.*, 2019, 19, 7185-7192.

6 J.-M. Chen, S. Li and T.-B. Lu, *Cryst. Growth Des*., 2014, 14, 6399-6408.

7 M. Yoshimura, M. Miyake, T. Kawato, M. Bando, M. Toda, Y. Kato, T. Fukami and T. Ozeki, *Cryst. Growth Des*., 2017, 17, 550-557.

8 J. Kastelic, Z. Hodnik, P. Sket, J. Plavec, N. Lah, I. Leban, M. Pajk, O. Planinsek and D. Kikelj, *Cryst. Growth Des*., 2010, 10, 4943-4953.

9 B. C. Dayo Owoyemi, C. C. da Silva, M. S. Souza, L. F. Diniz, J. Ellena and R. L. Carneiro, *Cryst. Growth Des*., 2019, 19, 648-657.